SECOND-ORDER EFFICIENT NONLINEAR FILTER STABILIZATION FOR HIGH REYNOLDS NUMBER FLOWS

AZIZ TAKHIROV *, CATALIN TRENCHEA †, AND JIAJIA WATERS ‡

Abstract. In this work, we develop a second-order nonlinear filter based stabilization scheme for high Reynolds number flows. We prove the unconditional stability of the method, establish the second order consistency and discuss the dynamical tuning of the relaxation parameter. The scheme is then validated against experimental data for an isothermal turbulent flow in a Staggered Tube Bundle at Reynolds number of 18000. Numerical results are found to be in an overall good qualitative and quantitative agreement with the benchmark results.

1. Introduction. When simulating a very high Reynolds number flow problem one is always faced with the lack of computational resources. One the one hand, fully resolving all the energetically significant scales in the flow down to the Kolmogorov micro-scale $\eta := \mathcal{O}\left(\mathrm{Re}^{-d/4}\right)$, $d = 2, 3$, [32] is impossible with the current computational power for many practical problems. On the other hand, underresolved simulations are known to produce unphysical flow structures (cf. [11, 29]), and non-physical solutions. These factors have motivated the development of many different methods for stabilizing underresolved flows.

One category of such methods, particularly suited for legacy codes, is the (nonlinear) adaptive filtering scheme of [27]. It was developed as an improvement to the linear filtering based stabilization schemes [10, 30, 13]. The basic idea behind the linear filtering is:

Given a result of underresolved simulation step

$$\begin{aligned} \frac{w^{n+1}-u^n}{\tau} + (u^n \cdot \nabla)\, w^{n+1} + \nabla p^{n+1} - \nu \Delta w^{n+1} &= 0 \\ \nabla \cdot w^{n+1} &= 0 \end{aligned} \tag{1.1}$$

apply a postprocessing linear Helmholtz filtering to remove the scales below the current mesh size h:

$$-h^2 \Delta \overline{w^{n+1}} + \overline{w^{n+1}} = w^{n+1}, \tag{1.2}$$

and perform a relaxation step:

$$u^{n+1} = (1-\chi)\overline{w^{n+1}} + \chi \overline{w^{n+1}}, \ 0 \le \chi = \chi_0 \tau \le 1, \chi_0 = \mathcal{O}(1). \tag{1.3}$$

Even though the idea allows for a modular implementation, the linear filtering and relaxation steps (1.2)-(1.3) distort the laminar parts of the flow as well, thereby resulting in lower accuracy. The main novelty of [27] was to adaptively tune the local filtering radius so that

$$\text{microscale} = \text{filter radius} = \text{spatial mesh-width}. \tag{1.4}$$

The adaptivity is achieved through the use of a nonlinear indicator function, $0 \le a(u, p, f) \le 1$, discussed in more detail in Section 2. All the adaptive/nonlinear filtering methods preserve the modular aspect of their linear counterparts, and thus can be easily integrated into the existing legacy codes. Second-order extension of [27] was further developed in [26], while new class of indicator functions were studied in [9, 28]. Solving the system (1.1)-(1.3) can be viewed as equivalent to implementing a Large Eddy Simulation (LES) [18, 5] model with an appropriate turbulent viscosity coefficient [31]. Thus, besides having a modular implementation, the adaptive filtering has a physical justification behind it, at least for flows at statistical equilibrium [7, 22, 23].

However, there are some computational drawbacks of the filtering equation (1.2), as were observed in [1]:

* (Corresponding author) Department of Mathematics, University of Sharjah, UAE. email: atakhirov@sharjah.ac.ae.

† Department of Mathematics, University of Pittsburgh, USA. email: trenchea@pitt.edu.

‡ Los Alamos National Laboratory, USA. email: waters@lanl.gov.

i) Unlike the Helmholtz filter (i.e., equation (1.2)) the Step 2 requires the assembly of the matrix at each time step.
ii) (1.1) is often solved via decoupling the velocity and the pressure variables, e.g. [17, 16, 15], which replaces the large linear system with two smaller ones. Then it is preferable and more efficient to have a post-processing step that does not require solving a mixed problem.

These observations led to the development of a more efficient adaptive stabilization model in [1], which has first order temporal accuracy. The first goal of the manuscript is to extend the analytical foundations of the first order scheme to second order one via multi-step BDF2 time discretization and prove its unconditional stability. Secondly, we also propose a new approach for tuning the proportionality constant χ_0 in (1.3). Finally, we also test our scheme on a widely used Staggered Tube Bundle problem at Re = 18000 in 2D, for which the experimental data is available, cf. [36, 37].

The numerical testing of the nonlinear filtering schemes have been restricted to mostly academic flow problems, with a notable exception being the three-dimensional Re = 5000 FDA Nozzle Benchmark study of [6]. The adaptive filtering [27] has also been synthesized with the Leray-α model in [8]. The idea has recently been applied to stabilize the instabilities in steady-state flow simulations ([39]) and fixing the backflow instabilities ([40]).

This paper is organized as follows. In Section 2, we present the notations, the choice of an indicator function, our numerical algorithm and recall the properties of the new adaptive filtering step. In Section 3, we establish the stability of the scheme, discuss its consistency and the dynamic selection of χ_0. Section 4 will be dedicated to numerical tests and the last Section will be the conclusion.

2. Preliminaries.

2.1. Notations. We denote by Ω an open, simply connected domain with piecewise smooth boundary. We denote the boundary of the domain by Γ.

The $L^2(\Omega)$ norm and inner product will be denoted by $\|\cdot\|$ and $(\cdot,\cdot)$. For simplicity of the presentation, we assume a no-slip boundary condition. In this setting, the appropriate velocity and pressure spaces are defined as

$$X := (H_0^1(\Omega))^d,\ Q := L_0^2(\Omega).$$

We use as the norm on X , $\|v\|_X := \|\nabla v\|_{L^2}$. The space of divergence free functions, and the standard $\mathrm{H}_{\mathrm{div}}(\Omega)$ space are given by

$$V := \{v \in X :\ (\nabla \cdot v, q) = 0\ \ \forall q \in Q\}$$
$$\mathrm{H}_{\mathrm{div}}(\Omega) := \left\{v \in L^2(\Omega)^d : \|v\|_{H_{div}} := \sqrt{\|v\|^2 + \|\nabla \cdot v\|^2} < \infty\right\},$$

respectively.

We will study the flow problems in $\Omega \times [0,T]$ cylinder domain. For a timestep Δt, we set $N = \frac{T}{\Delta t}$. Given sequence of functions $\{\phi^n\}_{n=1}^N \subset X$, and an indicator function $0 \le a(\cdot) \le 1$, we define the following quantities

$$\|\nabla w\|_{a^n} := \|\sqrt{a(\phi^n)}\nabla w\|,\quad \|\Delta_{a^n} w\|_* := \sup_{v\in X} \frac{(a(\phi^n)\nabla w, \nabla v)}{\|v\|},\quad 1 \le n \le N,$$

and

$$H_n^*(\Omega) := \{w \in X : \|\Delta_{a^n} w\|_* < \infty\},\quad 1 \le n \le N.$$

We also define

$$l^2(0,T;H^*(\Omega)) := \left\{\{w^n\}_{n=1}^N \subset X : \Delta t \sum_{n=1}^N \|\Delta_{a^n} w^n\|_*^2 < \infty\right\},$$

and

$$\|w\|_{l^2(0,T;H^*(\Omega))} := \sqrt{\Delta t \sum_{n=1}^{N} \|\Delta_{a^n} w^n\|_*^2}.$$

In order to alleviate the notation, throughout the analysis, we will assume that the discretization is continuous in space.

2.2. Indicator function. The indicator function $a(u,p,f)$ must be constructed so that

$$\begin{gathered} 0 \le a(\cdot) \le 1 \text{ at any point } (x,t), \\ a(\cdot) \simeq 0 \text{ selects regions requiring no local filtering,} \\ a(\cdot) \simeq 1 \text{ selects regions requiring } O(\delta) \text{ local filtering.} \end{gathered}$$

Several indicator functions have been proposed in the literature. [27] lists few phenomenology based indicator functions, while in [6] the authors consider mathematical one. In this work, we use the energy residual (entropy) based indicator function, inspired from [14, 19]. To this end, consider the numerical residual of the energy (entropy) equation as

$$D(x,t) := \frac{\partial_t}{2}|u|^2 + \nabla \cdot \left(\left(\frac{|u|^2}{2} + p \right) u \right) - \frac{\nu}{2}\Delta|u|^2 + \nu|\nabla u|^2 - f \cdot u.$$

When u and p are smooth enough, $D(x,t)$ is the residual of the momentum equation tested with u. As discussed in [14, 19], if $D(x,t) \le 0$ at a point (x,t) means that the energy is cascading down there and no additional dissipation is needed. In practice, one needs to ensure that $|D(x,t)| \ll 1$ and numerical dissipation is necessary where $|D(x,t)|$ is large. Using $D(x,t)$, we can construct an indicator function as follows

$$a_{EV}(u,p,f) = \frac{|D(x,t)|}{\max\left(\|D\|_{L^\infty(\Omega)}, 1\right)}.$$

2.3. Numerical algorithm. The scheme studied in [1] was first order, while in this work we consider its second order extension. For technical reasons, the grad-div term is added in the filtering equation:

ALGORITHM 2.1. *Given a forcing $f \in L^\infty(0,T;H^{-1}(\Omega))$, an initial velocity u_0, a timestep $\tau > 0$, filter radius δ, endtime T, $u^{*,n+1} = 2u^n - u^{n-1}$ and integer N satisfying $T = N\tau$, find (u^{n+1}, p^{n+1}) satisfying*

Step 1:
$$\frac{3w^{n+1} - 4u^n + u^{n-1}}{2\tau} + \left(u^{*,n+1} \cdot \nabla\right) w^{n+1} + \nabla \hat{p}^{n+1} - \nu\Delta w^{n+1} = f(t^{n+1}) \tag{2.1}$$
$$\nabla \cdot w^{n+1} = 0 \tag{2.2}$$

Step 2:
$$-\delta^2 \Delta \overline{w^{n+1}} + \overline{w^{n+1}} - \nabla\nabla \cdot \overline{w^{n+1}} + \nabla\lambda^{n+1}$$
$$-\delta^2 \nabla \cdot (a(w^{n+1})\nabla \overline{w^n}) - \delta^2 \Delta \overline{w^n} = w^{n+1} \tag{2.3}$$
$$\lambda^{n+1} - \lambda^n + \nabla \cdot \overline{w^{n+1}} = 0 \tag{2.4}$$

Step 3:
$$u^{n+1} = (1-\chi)w^{n+1} + \chi\overline{w^{n+1}} \tag{2.5}$$
$$p^{n+1} = (1-\chi)\hat{p}^{n+1} + \chi\lambda^{n+1}. \tag{2.6}$$

In the implementation of equation (2.3), λ^{n+1} is replaced by $\lambda^n - \nabla \cdot \overline{w^{n+1}}$, thereby decoupling the equations in Step 2.

2.4. Properties of the filter. In this section we are going to recall some of the properties of the filter (2.3)-(2.4) from [1], formulated for $\overline{w}^0 = \lambda^0 = 0$ case with the contribution of the new grad-div term taken into account.

LEMMA 2.2. *For an arbitrary sequence $\{\phi^n\}_{n=1}^N \subset X$, and a given $w(x,t) \in X$, $\forall t \in [0,T]$, let $w^n := w(x,t_n)$. Assume that $(\overline{w^n}, \lambda^n)$ is a sequence generated by the Step 2 of the Algorithm 2.1 with indicator functions $a(\phi^{n+1})$ instead of $a(w^{n+1})$. Then*

$$\delta^2 \|\nabla \overline{w^N}\|^2 + \sum_{n=0}^{N-1} \|\overline{w^{n+1}}\|_{H_{div}}^2 + \|\lambda^N\|^2 \leq \sum_{n=0}^{N-1} \|w^{n+1}\|^2, \tag{2.7}$$

$$\|\overline{w}\|_{\ell^2([0,T];H_{div}(\Omega))} \leq \|w\|_{\ell^2([0,T];L^2(\Omega))}, \tag{2.8}$$

$$(w, \overline{w})_{\ell^2([0,T];L^2(\Omega))} \geq 0, \tag{2.9}$$

and

$$(w - \overline{w}, \overline{w})_{\ell^2([0,T];L^2(\Omega))} \geq 0. \tag{2.10}$$

The error in proposed nonlinear filtering step can be estimated as follows:

LEMMA 2.3. *For an arbitrary sequence $\{\phi^n\}_{n=1}^N \subset X$, and a given $w(x,t)$ belonging to $L^\infty([0,T];V) \cap l^2(0,T;H^*(\Omega))$, with $w_t \in L^2\left([0,T];H^2(\Omega)\right)$, let $w^n := w(x,t_n)$. Assume that $(\overline{w^n}, \lambda^n)$ is a sequence generated by the Step 2 of the Algorithm 2.1 with indicator functions $a(\phi^{n+1})$.*

Let $e^n := w(x,t_n) - \overline{w_n}$ be the filtering error at time t_n. Then

$$\delta^2 \|\nabla e^N\|^2 + \sum_{n=0}^{N-1} \|e^{n+1}\|_{H_{div}}^2 + \|\lambda^N\|^2 \leq C\left(\delta^4 + \frac{\delta^4}{\tau}\right), \tag{2.11}$$

$$\|e\|_{l^2\left(0,T;_{H_{div}}(\Omega)\right)} \leq C\left(\delta^2\tau + \delta^2\right). \tag{2.12}$$

3. Theoretical results.

3.1. Stability. We let $f = 0$ for simplicity. A crucial ingredient in the stability proof will be the following equation from [1, equation (19)], appropriately reformulated here for the modified filter:

$$\begin{aligned} &\frac{\delta^2}{2}\left(\left\|\nabla\overline{w^{n+1}}\right\|^2 - \left\|\nabla\overline{w^n}\right\|^2\right) + \frac{\delta^2}{2}\left\|\sqrt{1-a(w^{n+1})}\nabla(\overline{w^{n+1}} - \overline{w^n})\right\|^2 \\ &\quad + \frac{\delta^2}{2}\left(\left\|\nabla\overline{w^{n+1}}\right\|_{a^{n+1}}^2 + \left\|\nabla\overline{w^n}\right\|_{a^{n+1}}^2\right) + \|\nabla\cdot\overline{w^{n+1}}\|^2 \\ &\quad + \frac{\|\lambda^{n+1}\|^2 - \|\lambda^n\|^2 + \|\lambda^{n+1} - \lambda^n\|^2}{2} = \left(w^{n+1} - \overline{w^{n+1}}, \overline{w^{n+1}}\right). \end{aligned} \tag{3.1}$$

THEOREM 3.1. *Assume that $\chi \le 1$ and $t \in (0,T]$. Define the system energy and dissipation by*

$$\begin{aligned} E^{n+1} :=& \frac{\|u^{n+1}\|^2 + \|2u^{n+1}-u^n\|^2}{4} + \frac{3\chi}{4}\delta^2\|\nabla\overline{w^{n+1}}\|^2 \\ &+ \frac{\chi(1-\chi)}{2}\left\|w^{n+1}-\overline{w^{n+1}}\right\|^2 + \frac{\chi}{2}\|\lambda^{n+1}\|^2 + \chi\left\|\nabla\cdot\overline{w^{n+1}}\right\|^2 \end{aligned} \tag{3.2}$$

$$\begin{aligned} D^{n+1} :=& \frac{\|u^{n+1}-2u^n+u^{n-1}\|^2}{8\tau} + \frac{\left\|u^{n+1}-2u^n+u^{n-1}+2\chi(w^{n+1}-\overline{w^{n+1}})\right\|^2}{4} \\ &+ \nu\|\nabla w^{n+1}\|^2 + \chi\frac{3-\chi}{2\tau}\|w^{n+1}-\overline{w^{n+1}}\|^2 \\ &+ \frac{5\chi\delta^2}{4\tau}\left\|\nabla\overline{w^{n+1}}\right\|_{a^{n+1}}^2 + \frac{\chi}{\tau}\left(\left\|\nabla\cdot\left(w^{n+1}-\overline{w^{n+1}}\right)\right\|^2 + \frac{\left\|\nabla\cdot w^{n+1}\right\|^2}{8}\right). \end{aligned} \tag{3.3}$$

Then for any choice of the time step $\tau > 0$, the Algorithm 2.1 is unconditionally stable and satisfies

$$E^N + \tau\sum_{n=1}^{N-1} D^{n+1} \le |E^1| + 2\chi\tau\left|\left(\nabla\cdot\overline{w^1}, \lambda_1\right)\right|. \tag{3.4}$$

Proof. Multiply (2.1) by w^{n+1} and (2.2) by $\hat{p}^{n+1}$, and add the resulting equations to get

$$\frac{\left(3w^{n+1}-4u^n+u^{n-1}, w^{n+1}\right)}{2\tau} + \nu\|\nabla w^{n+1}\|^2 = 0. \tag{3.5}$$

The first term in (3.5), ignoring the denominator, can be decomposed as

$$\begin{aligned} \left(3w^{n+1}-4u^n+u^{n-1}, w^{n+1}\right) &= 3\left(w^{n+1}-u^{n+1}, w^{n+1}\right) + \left(3u^{n+1}-4u^n+u^{n-1}, w^{n+1}\right) \\ &= 3\left(w^{n+1}-u^{n+1}, w^{n+1}\right) + \left(3u^{n+1}-4u^n+u^{n-1}, u^{n+1}\right) \\ &+ \left(3u^{n+1}-4u^n+u^{n-1}, w^{n+1}-u^{n+1}\right) \\ &=: I_1 + I_2 + I_3. \end{aligned} \tag{3.6}$$

Using the fact that $w^{n+1}-u^{n+1} = \chi\left(w^{n+1}-\overline{w^{n+1}}\right)$, (3.1), and (2.4), we obtain that

$$\begin{aligned} I_1 &= 3\chi\left(w^{n+1}-\overline{w^{n+1}}, w^{n+1}\right) \\ &= 3\chi\left\|w^{n+1}-\overline{w^{n+1}}\right\|^2 + 3\chi\left(w^{n+1}-\overline{w^{n+1}}, \overline{w^{n+1}}\right) \\ &= 3\chi\left\|w^{n+1}-\overline{w^{n+1}}\right\|^2 \\ &+ \frac{3\chi}{2}\delta^2\left[\left\|\nabla\overline{w^{n+1}}\right\|^2 - \left\|\nabla\overline{w^n}\right\|^2 + \left\|\sqrt{1-a(w^{n+1})}\nabla(\overline{w^{n+1}}-\overline{w^n})\right\|^2\right. \\ &\left.+\left\|\nabla\overline{w^{n+1}}\right\|_{a^{n+1}}^2 + \left\|\nabla\overline{w^n}\right\|_{a^{n+1}}^2\right] \\ &+ \frac{3\chi}{2}\left(\frac{3}{2}\left\|\nabla\cdot\overline{w^{n+1}}\right\|^2 + \|\lambda^{n+1}\|^2 - \|\lambda^n\|^2\right). \end{aligned} \tag{3.7}$$

Thanks to the standard polarization identity for BDF2, we get that

$$\begin{aligned} I_2 =& \frac{\|u^{n+1}\|^2 + \|2u^{n+1}-u^n\|^2 - \|u^n\|^2 - \|2u^n-u^{n-1}\|^2}{2} \\ &+ \frac{\|u^{n+1}-2u^n+u^{n-1}\|^2}{2}. \end{aligned} \tag{3.8}$$

It remains to deal with I_3 term, which turns out to be not so straightforward. Again using the equality $w-u=\chi\left(w-\overline{w}\right)$, we get that

$$\begin{aligned} I_3 &= \left(3u^{n+1}-4u^n+u^{n-1}, w^{n+1}-u^{n+1}\right) = \left(3u^{n+1}-4u^n+u^{n-1}, \chi\left(w^{n+1}-\overline{w^{n+1}}\right)\right) \\ &= \chi\left(u^{n+1}-2u^n+u^{n-1}, w^{n+1}-\overline{w^{n+1}}\right)+2\chi\left(u^{n+1}-u^n, w^{n+1}-\overline{w^{n+1}}\right) \\ &:= I_{31}+I_{32}. \end{aligned} \tag{3.9}$$

Using the identity

$$(a,\chi b)=\left(\frac{a}{\sqrt{2}},\sqrt{2}\chi b\right)=-\frac{a^2}{4}-\chi^2b^2+\frac{(a+2\chi b)^2}{4},$$

the I_{31} term in (3.9) can written as

$$\begin{aligned} I_{31} = &-\frac{\left\|u^{n+1}-2u^n+u^{n-1}\right\|^2}{4}-\chi^2\left\|w^{n+1}-\overline{w^{n+1}}\right\|^2 \\ &+\frac{\left\|u^{n+1}-2u^n+u^{n-1}+2\chi(w^{n+1}-\overline{w^{n+1}})\right\|^2}{4}. \end{aligned} \tag{3.10}$$

The first term in (3.10) will be controlled by the last term in (3.8), while its second term will be majorized by the first term of (3.7).

It remains to bound the I_{32} term. Upon rewriting (2.5) as

$$u=(1-\chi)w+\chi\overline{w}=(1-\chi)(w-\overline{w})+\overline{w},$$

we obtain that

$$\begin{aligned} I_{32} &= 2\chi\left(u^{n+1}-u^n, w^{n+1}-\overline{w^{n+1}}\right) \\ &= 2\chi(1-\chi)\left(\left(w^{n+1}-\overline{w^{n+1}}\right)-\left(w^n-\overline{w^n}\right), w^{n+1}-\overline{w^{n+1}}\right) \\ &+2\chi\left(\overline{w^{n+1}}-\overline{w^n}, w^{n+1}-\overline{w^{n+1}}\right) \\ &= \frac{\left\|w^{n+1}-\overline{w^{n+1}}\right\|^2-\left\|w^n-\overline{w^n}\right\|^2+\left\|\left(w^{n+1}-\overline{w^{n+1}}\right)-\left(w^n-\overline{w^n}\right)\right\|^2}{2} \\ &+\underbrace{2\chi\left(\overline{w^{n+1}}-\overline{w^n}, w^{n+1}-\overline{w^{n+1}}\right)}_{:=I_4}. \end{aligned} \tag{3.11}$$

The I_4 term is the most problematic term, and it will be bounded through the filtering equation (2.4) as follows:

$$\begin{aligned} I_4 &= 2\chi\left(\overline{w^{n+1}}-\overline{w^n}, -\delta^2\Delta\left(\overline{w^{n+1}}-\overline{w^n}\right)-\delta^2\nabla\cdot\left(a(w^{n+1})\nabla\overline{w^n}\right)-\nabla\nabla\cdot\overline{w^{n+1}}+\nabla\lambda^{n+1}\right) \\ &= 2\chi\delta^2\left[\left\|\nabla\left(\overline{w^{n+1}}-\overline{w^n}\right)\right\|^2+\frac{\left\|\nabla\overline{w^{n+1}}\right\|_{a^{n+1}}^2-\left\|\nabla\overline{w^n}\right\|_{a^{n+1}}^2-\left\|\nabla\left(\overline{w^{n+1}}-\overline{w^n}\right)\right\|_{a^{n+1}}^2}{2}\right] \\ &+\chi\left(\left\|\nabla\cdot\overline{w^{n+1}}\right\|^2-\left\|\nabla\cdot\overline{w^n}\right\|^2+\left\|\nabla\cdot\left(\overline{w^{n+1}}-\overline{w^n}\right)\right\|^2\right) \\ &\underbrace{-2\chi\left(\nabla\cdot\left(\overline{w^{n+1}}-\overline{w^n}\right), \lambda^{n+1}\right)}_{:=I_{41}} \end{aligned} \tag{3.12}$$

Notice that the first term in the second line of (3.12) dominates the last term there, while the other two terms of the same line will be controlled by the last term in line 5 of (3.7). The I_{41} term can be expressed as telescoping terms plus a negative contribution:

$$\begin{aligned} I_{41} &= -2\chi\left(\nabla\cdot\left(\overline{w^{n+1}}-\overline{w^n}\right),\lambda^{n+1}\right)\\ &= -2\chi\left[\left(\nabla\cdot\overline{w^{n+1}},\lambda^{n+1}\right)-\left(\nabla\cdot\overline{w^n},\lambda^n\right)\right]+2\chi\left(\nabla\cdot\overline{w^n},\underbrace{\lambda^{n+1}-\lambda^n}_{=-\nabla\cdot\overline{w^{n+1}}}\right)\\ &= -2\chi\left[\left(\nabla\cdot\overline{w^{n+1}},\lambda^{n+1}\right)-\left(\nabla\cdot\overline{w^n},\lambda^n\right)\right]\\ &\quad-\chi\left(\left\|\nabla\cdot\overline{w^{n+1}}\right\|^2+\left\|\nabla\cdot\overline{w^n}\right\|^2-\left\|\nabla\cdot\left(\overline{w^{n+1}}-\overline{w^n}\right)\right\|^2\right) \end{aligned} \tag{3.13}$$

Combining (3.13) with (3.12), we arrive at

$$\begin{aligned} I_4 &= 2\chi\delta^2\left[\left\|\nabla\left(\overline{w^{n+1}}-\overline{w^n}\right)\right\|^2+\frac{\left\|\nabla\overline{w^{n+1}}\right\|_{a^{n+1}}^2-\left\|\nabla\overline{w^n}\right\|_{a^{n+1}}^2-\left\|\nabla\left(\overline{w^{n+1}}-\overline{w^n}\right)\right\|_{a^{n+1}}^2}{2}\right]\\ &\quad+2\chi\left(\left\|\nabla\cdot\overline{w^{n+1}}\right\|^2-\left\|\nabla\cdot\overline{w^n}\right\|^2+\left\|\nabla\cdot\left(\overline{w^{n+1}}-\overline{w^n}\right)\right\|^2\right)-2\chi\left\|\nabla\cdot\overline{w^{n+1}}\right\|^2\\ &\quad-2\chi\left[\left(\nabla\cdot\overline{w^{n+1}},\lambda^{n+1}\right)-\left(\nabla\cdot\overline{w^n},\lambda^n\right)\right]. \end{aligned} \tag{3.14}$$

The bothering $-2\chi\left\|\nabla\cdot\overline{w^{n+1}}\right\|^2$ term in (3.14) is controlled by a similar term in (3.7), leaving a positive term $\frac{\chi}{4}\left\|\nabla\cdot\overline{w^{n+1}}\right\|^2$.

Putting together all the expressions we have obtained for $I_j, j=1,2,3,4$ with (3.5), and dropping some non-essential positive terms yields

$$\begin{aligned} &\widetilde{E}^{n+1}-\widetilde{E}^n+\tau D^{n+1}+\frac{3\chi}{2}\left(\|\lambda^{n+1}\|^2-\|\lambda^n\|^2\right)+2\chi\left(\|\nabla\cdot\overline{w^{n+1}}\|^2-\|\nabla\cdot\overline{w^n}\|^2\right)\\ &\qquad\le 2\chi\left[\left(\nabla\cdot\overline{w^{n+1}},\lambda^{n+1}\right)-\left(\nabla\cdot\overline{w^n},\lambda^n\right)\right], \end{aligned} \tag{3.15}$$

where $\widetilde{E}^{n+1}=E^{n+1}-\frac{\chi}{2}\|\lambda^{n+1}\|^2-\chi\|\nabla\cdot\overline{w}^{n+1}\|^2$. Now sum over the timesteps n from $n=1$ to $n=N-1$ to get

$$\begin{aligned} &E^N+\tau\sum_{n=1}^{N-1}D^{n+1}+\frac{3\chi}{2}\|\lambda^N\|^2+2\chi\|\nabla\cdot\overline{w^N}\|^2\\ &\qquad\le|E^1|+2\chi\left|\left(\nabla\cdot\overline{w^1},\lambda^1\right)\right|+\chi\left(\|\lambda^N\|^2+\|\nabla\cdot\overline{w^N}\|^2\right). \end{aligned} \tag{3.16}$$

Thus the last two terms in (3.16) are controlled by the corresponding terms in the left hand side, and the proof is therefore complete. □

3.2. Consistency. At a time-continuous level, the Algorithm 1 is equivalent to performing an eddy viscosity model with a Voigt regularization. To see this, rewrite the Step 1 as

$$\begin{aligned} &\frac{3u^{n+1}-4u^n+u^{n-1}}{2\tau}+\left(u^{*,n+1}\cdot\nabla\right)w^{n+1}+\nabla\hat{p}^{n+1}\\ &\qquad-\nu\Delta w^{n+1}+\frac{3(w^{n+1}-u^{n+1})}{2\tau}=f(t^{n+1}). \end{aligned} \tag{3.17}$$

Steps 2 and 3 imply

$$w^{n+1} - u^{n+1} = \chi(w^{n+1} - \overline{w^{n+1}}) \tag{3.18}$$
$$= \chi\left(-\delta^2\Delta(\overline{w^{n+1}} - \overline{w^n}) - \delta^2\nabla\cdot(a(w^{n+1})\nabla\overline{w^n}) - \nabla\nabla\cdot\overline{w^{n+1}} + \nabla\lambda^{n+1}\right).$$

Combining the last two equations, we obtain

$$\frac{3u^{n+1} - 4u^n + u^{n-1}}{2\tau} + \left(u^{*,n+1}\cdot\nabla\right)w^{n+1} + \nabla\left(\hat{p}^{n+1} + \frac{3\chi}{2\tau}\lambda^{n+1}\right) - \nu\Delta w^{n+1} \tag{3.19}$$
$$+ \frac{3\chi}{2\tau}\left(-\delta^2\Delta(\overline{w^{n+1}} - \overline{w^n}) - \delta^2\nabla\cdot(a(w^{n+1})\nabla\overline{w^n}) - \nabla\nabla\cdot\overline{w^{n+1}}\right) = f(t^{n+1}).$$

The stability and convergence analyses [27, 1] dictate that $\chi = \chi_0\tau$, which indicates that the Algorithm is overall second order consistent. Note that $\nabla\cdot u$ is also computed to the formal second order accuracy in time, as a consequence of a simple application of the triangle inequality on (2.4):

$$\left\|\nabla\cdot u\right\| \le (1-\chi)\underbrace{\left\|\nabla\cdot w\right\|}_{\text{2nd order from (2.2)}} + C\tau\underbrace{\left\|\nabla\cdot\overline{w}\right\|}_{\text{1st order from (2.4)}}.$$

The convergence test in Numerical tests section with a manufactured solution does indeed produce second order results.

The corresponding model PDE of (3.17) is then given by:

$$\partial_t u + u\cdot\nabla u + \nabla\left(\hat{p} + \frac{3\chi}{2\tau}\lambda\right) - \nu\Delta u - \frac{3\chi}{2\tau}\delta^2\nabla\cdot(a(u)\nabla u) - \frac{3\chi}{2}\delta^2\Delta\partial_t u = f \tag{3.20}$$
$$\nabla\cdot u = 0. \tag{3.21}$$

The last term on the left hand side can be readily recognized as the Voigt regularization term of order $\mathcal{O}(\delta^2\tau)$, and therefore the time-relaxation [12, 38] introduced by it should be negligible. The next-to-last term can be recognized as an turbulent diffusion term with the turbulent viscosity coefficient $\nu_T = \frac{3\chi}{2\tau}\delta^2 a(u)$.

3.3. End-of-step pressure. The optimal choice of the end-of-step pressure p is still an open question. On the one hand, simply picking $p = \hat{p}$ would be clearly inefficient, as it corresponds to an underresolved step. On the other hand, the equation (3.20) suggest that

$$p = \hat{p} + \frac{3\chi}{2\tau}\lambda.$$

However, the numerical tests demonstrated that such choice would also produce inaccurate pressure approximation. For this reason, we simply update the pressure in the same way as the velocity variable using (2.6).

3.4. On the choice of relaxation parameter χ. The established formal stability and convergence results indicate that $\chi = \chi_0\tau$ for some $\chi_0 > 0$. For academic test problems, choosing $\chi_0 = 1$ has been found to work well. However, as was noted in [6, pg. 474], in practical problems this choice does not provide enough numerical dissipation, which we also experienced.

In order to dynamically pick χ_0, consider (3.20). Define the effective viscosity coefficient and the corresponding effective Reynolds number:

$$\nu_{eff} := \nu + \frac{3\chi_0}{2}\delta^2 a(u) \text{ and } \mathrm{Re}_{eff} := \frac{\mathrm{UL}}{\nu_{eff}}.$$

Now assuming that mesh diameter h is greater than the Kolmogorov scale η, the goal is to pick χ_0 so that the equation (1.4) is enforced for the effective Kolmogorov mircoscale

$$h = \eta_{eff} \simeq \mathrm{Re}_{eff}^{-d/4}.$$

Thus we get

$$h \simeq \mathrm{Re}_{eff}^{-d/4} \simeq \mathrm{Re}^{-d/4} \left(\frac{\nu}{\nu_{eff}}\right)^{-d/4} \simeq \eta \left(\frac{\nu}{\nu_{eff}}\right)^{-d/4} \Longrightarrow$$

$$\chi_0^n \simeq \min\left(\frac{2\nu}{3\delta^2\|a(w^n)\|}\left(\left(\frac{h}{\eta}\right)^{4/d} - 1\right), \frac{1}{\tau}\right). \tag{3.22}$$

This gives slightly larger amount of numerical dissipation compared to that of [6]:

$$\chi_0^n \simeq \min\left(\frac{2\nu}{3\delta^2\|a(w^n)\|}\left(\frac{h}{\eta} - 1\right), \frac{1}{\tau}\right).$$

In our simulations presented below, we used h_{min} as the value of the filtering radius δ in (3.22). However when solving (2.3), δ was picked as the local element diameter.

4. Numerical Experiments. In this section, we present several numerical experiments that demonstrate the effectiveness of our algorithm and the entropy based indicator function, in giving good coarse mesh approximations for flow problems. We used $P_2 - P_1$ Taylor-Hood element pair [2] for the space approximations. All the tests below are performed using the FreeFem++ package [21].

4.1. Convergence Study. Next we present the convergence results. In order to test the overall second-order accuracy of our solution, we use a manufactured solution

$$\begin{aligned} u_1 &= \sin(2\pi x)\sin(2\pi(y+t)), \\ u_2 &= \cos(2\pi x)\cos(2\pi(y+t)), \\ p &= \cos(2\pi x)\sin(2\pi(y+t)), \\ f &= u_t + u\cdot\nabla u - \nu\Delta u + \nabla p. \end{aligned}$$

The domain is taken to be a unit square. We refine both the mesh size and the timestep τ. The viscosity is taken to be $\nu = 1$ and the relaxation parameter is kept constant $\chi = \tau$.

The final time is $T = 1$. The timestep Δt is halved for each successive run starting with $\tau t = 0.01$. The Table 4.1 and the Figure 4.1 confirm the expected convergence rates.

Table 4.1: Errors in various norms

dt	$\|e^N\|$	$\|\nabla e\|_{l^2([0,T];L^2(\Omega))}$	$\|\nabla\cdot e^N\|$	$\|e_p^N\|$
0.01	5.697112e-3	2.439626e-1	1.652136e-1	3.859639e-2
0.005	1.264310e-3	6.249729e-2	4.367814e-2	9.271334e-3
0.0025	3.104765e-4	1.587989e-2	1.110705e-2	2.729526e-3
0.00125	7.759817e-5	3.992630e-3	2.790654e-3	8.342931e-4

4.2. Tube Bundle Benchmark. In this subsection, we will present our results for two dimensional flow over simplified staggered tube bundle array. The geometry of the flow domain is similar to the lower plenum of a gas-cooled high temperature reactor. The actual experimental test section consists of uniformly placed staggered rows of rods with a pitch of 45 mm, across which water flows at an average velocity of U = 1.06 m/s. With a tube diameter of L = 21.7 mm, the Reynolds number is 18000. LDA measurements indicate that the flow becomes periodic around the fourth row from the bottom, which is taken often taken as the computational domain, Fig. 4.2, and is also adopted herein. More details of this experiment can be found at the European Research Community on Fluid, Turbulence and Combustion database (http://cfd.mace.manchester.ac.uk/ercoftac/doku.php?id=cases:case078).

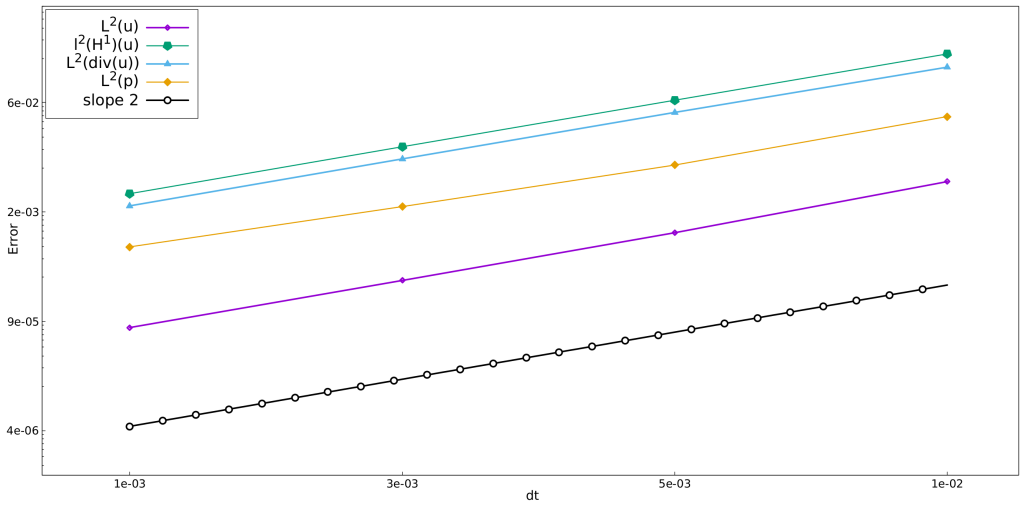

Fig. 4.1: Errors in logscale

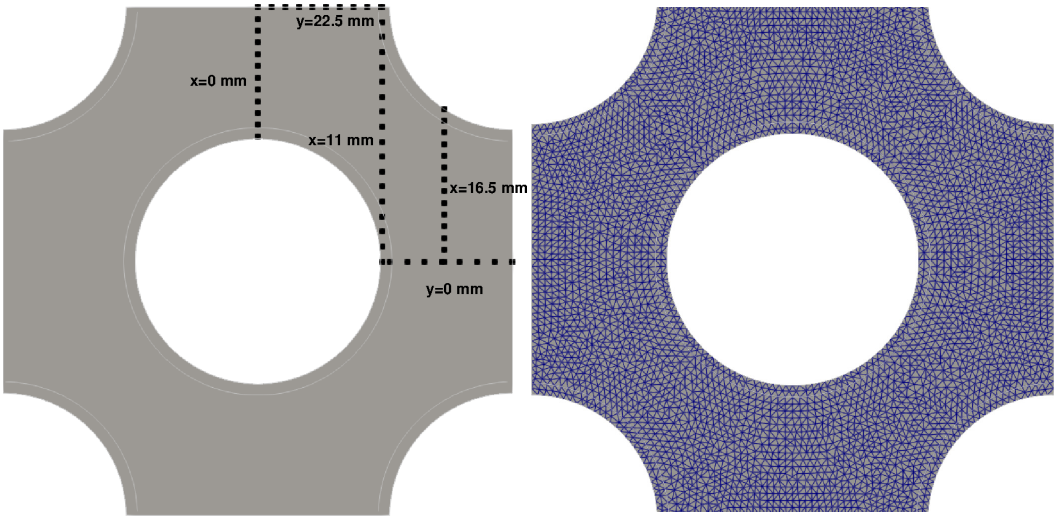

Fig. 4.2: Left: Computational domain centered at the origin, $|x|, |y| \leq 22.5$; Right: finite element mesh with 7734 elements

The works of Simonin & Barcouda [36, 37], and the accessible dataset are widely used as a benchmark for various CFD codes. Experimental data on (long-time averaged) mean velocities $\overline{u}, \overline{v}$ and Reynolds stresses $\overline{u'u'}$, $\overline{v'v'}$, $\overline{u'v'}$ are provided for three x and two y locations, specifically, $x = 0, 11, 16.5$ mm and $y = 0$ and $y = 22.5$ mm.

Most numerical studies of this problem were carried out in 3D, e.g., [3, 35, 20, 25], although some include a few preliminary runs of a 2D simulations as well. On the other hand, only a few articles are dedicated to a detailed 2D simulations of this problem. For instance, Ridluan and Tokuhiro have tested steady RANS equations with four different turbulence models, and obtained marginal to poor results [33]. In a companion work [34], they tested unsteady RANS equations with Reynolds Stress Model and obtained better agreement with the available dataset. Johnson [24] also used this problem to validate his 2D URANS model. All of these 2D works use the commercial CFD code FLUENT, special wall treatment and explicitly solve for Reynolds stresses using the Reynolds Stress Turbulence model.

We generate the initial velocity field from the discrete mean velocity profile of [37]. Specifically, the discrete data at the inlet is interpolated linearly, giving $\left(U^0(y), V^0(y)\right)^T$, and is used to generate the initial velocity field via solving the Stokes equation:

$$\begin{aligned} -\Delta u^0 + \nabla p^0 &= f(x) \text{ in } \Omega, \\ \nabla \cdot u^0 &= 0 \text{ in } \Omega, \\ u^0 &= \left(U^0(y), V^0(y)\right)^T \text{ at } x = -22.5 \text{ and } x = 22.5, \\ u^0 &= 0 \text{ at cylinder surfaces}, \\ u^0\big|_{y=-22.5} &= u^0\big|_{y=22.5}, \end{aligned}$$

where the right hand side function $f(x)$ is a random function with values in $[-0.01, 0.01]$. In this way, we generate incompressible initial velocity field with random perturbations.

The boundary conditions are taken to be periodic in x and y directions, and no slip on the cylinder surfaces. In order to maintain the mass flow rate in the system equal to its initial value, a mean streamwise pressure gradient term $F^{n+1}\overrightarrow{e}_1$ is added to the streamwise momentum equation (2.2) and is adjusted [4] at each time step as

$$F^{n+1} = F^n + \frac{1}{\tau}\left[m^0 - 2m^n + m^{n-1}\right], \tag{4.1}$$

where

$$m^0 = \int_{x=-22.5} u^0(x, y)dy$$

is the initial bulk velocity multiplied by the size of the inlet.

The simulations were ran until the flow reached a statistically steady state. Solutions were computed on two grids, the coarser grid on Fig. 4.2 has 7734 cells, while the finer grid has 23038 cells. The maximum difference for the mean streamwise velocity was less than 4% relative to the coarser grid. Time convergence tests were also performed, and it was observed that reducing τ had no major affect on the flow statistics. The current reported results are obtained with $\tau = 0.001$.

In what follows, we present the results performed on the coarse mesh. Figures 4.3 - 4.4 show the mean velocity components, and the mean pressure field. Qualitatively, we have an excellent agreement with the results of [34]. The instantaneous velocity field superimposed on the speed contours are shown in the Figure 4.5, which clearly demonstrate the flow instability in the wake of the central cylinder.

The predicted mean velocities are given in Figures 4.6-4.10. In those graphs, *NLF* stands nonlinear filtering and corresponds to the results found by our Algorithm, while S&B graphs are the experimental ones. Overall, the mean streamwise velocity results are in very good to excellent agreement with the experimental data.

Concerning the mean spanwise velocities, the data at x locations resembles the reference data well. It should be pointed out that, no published result matches the "zig-zag" pattern of experimental data at $x = 0$. Larger deviation is seen at y locations, which are also observed in [34, 24]. In fact, due to the symmetry of the truncated computational domain and the periodicity, the spanwise velocity should be zero at $y = 0$ and $y = 22.5$, which we actually have.

Symmetry arguments also dictate that the shear Reynolds stress term $\overline{u'v'}$ is zero at y locations, as observed in middle graphs of Figures 4.14 and 4.15. Overall, the graphs mimic the trend of the experimental data, except in a few instances, where the quality of the approximation is marginal. The remaining graphs of stresses are presented in Figures 4.11-4.13.

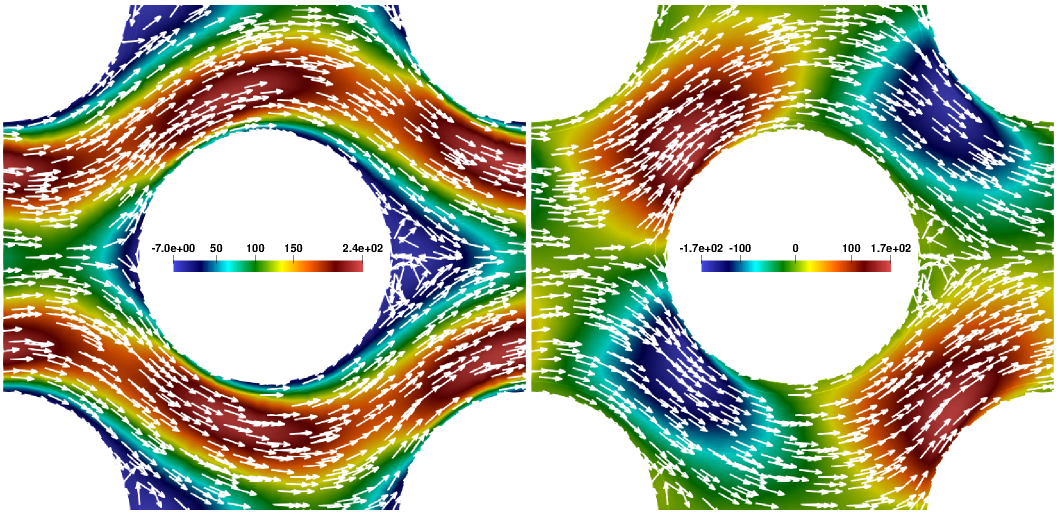

Fig. 4.3: x and y components of the mean velocity. Units are cm/s.

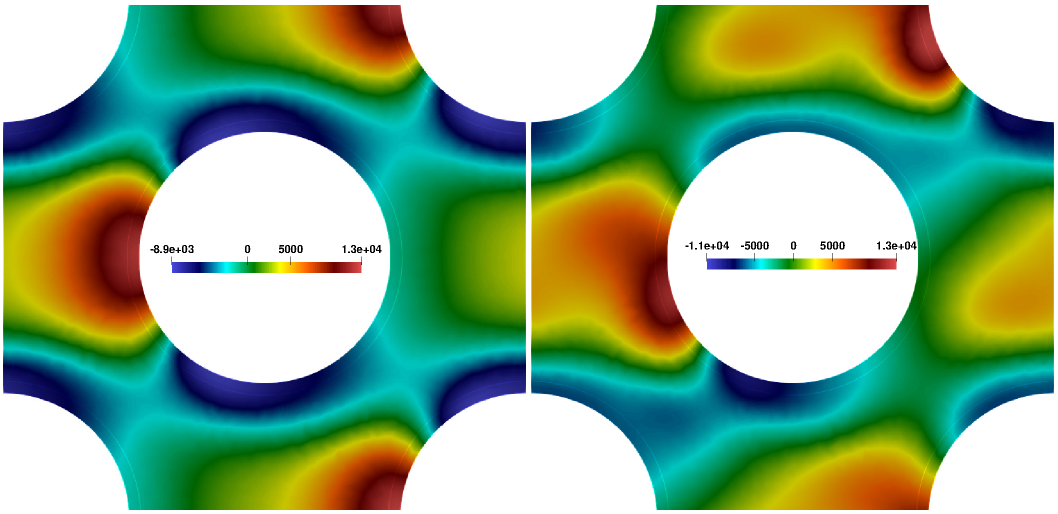

Fig. 4.4: Mean pressure (left) and instantaneous pressure (right) at $t = 1$. Units are $\mathrm{cm}^2/\mathrm{s}^2$.

5. Conclusions. We presented the second-order accurate extension of the efficient nonlinear stabilization scheme of [1]. The scheme is shown to be unconditionally stable and was tested on Tube Bundle flow problem at Re = 18000. Very coarse mesh was used, and no wall treatment was performed. Nonetheless, the qualitative results match the published ones well, while quantitatively the mean velocities profiles are also computed with good accuracy. Since the Tube Bundle flow is inherently a 3D flow, the accurate prediction of Reynolds stresses would probably require 3D simulations (cf. [3]) and a full length of the domain (cf. [20]).

Further studies will be performed for the nonlinear stabilization method to incorporate the wall treatment, and the backscatter, which also be tested on various benchmark problems. The sensitivity of the solution with respect to the relaxation constant χ will be also performed.

6. Acknowledgements. The first author would like acknowledge very helpful discussions with William Layton (University of Pittsburgh) and Traian Iliescu (Virginia Tech).

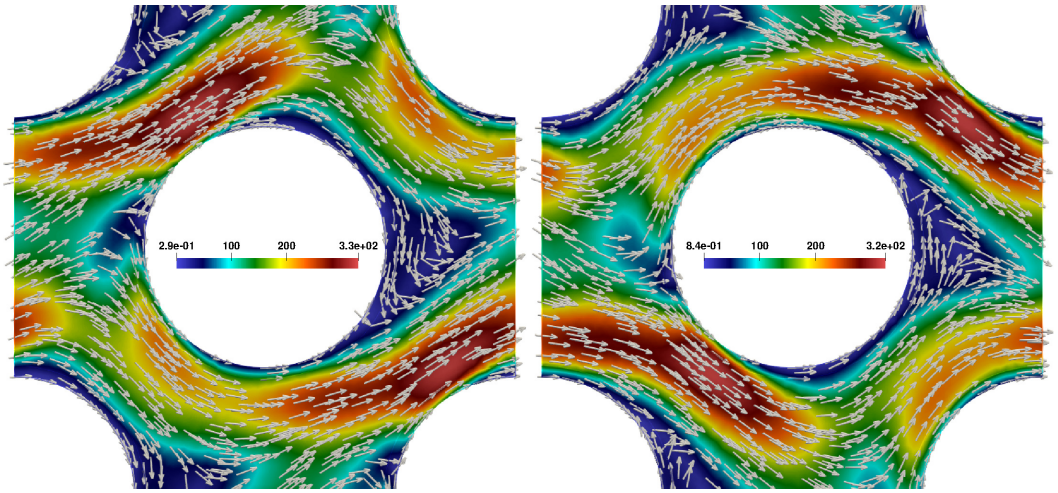

Fig. 4.5: Instantaneous speed contours at $t = 0.2$ and $t = 1$

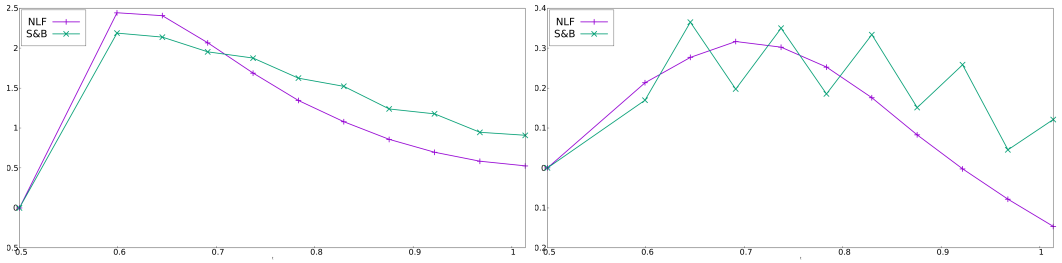

Fig. 4.6: Mean streamwise (left) and spanwise (right) velocity at $x = 0$

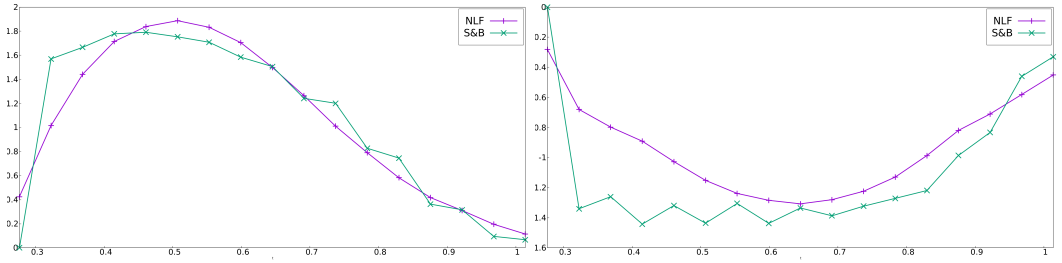

Fig. 4.7: Mean streamwise (left) and spanwise (right) velocity at $x = 11$

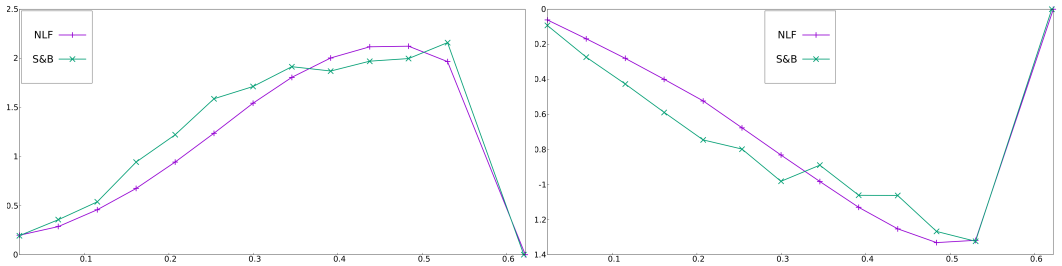

Fig. 4.8: Mean streamwise (left) and spanwise (right) velocity at $x = 16.5$

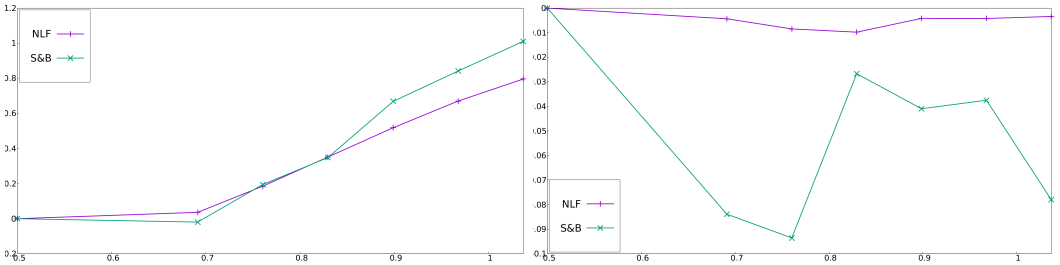

Fig. 4.9: Mean streamwise (left) and spanwise (right) velocity at $y = 0$

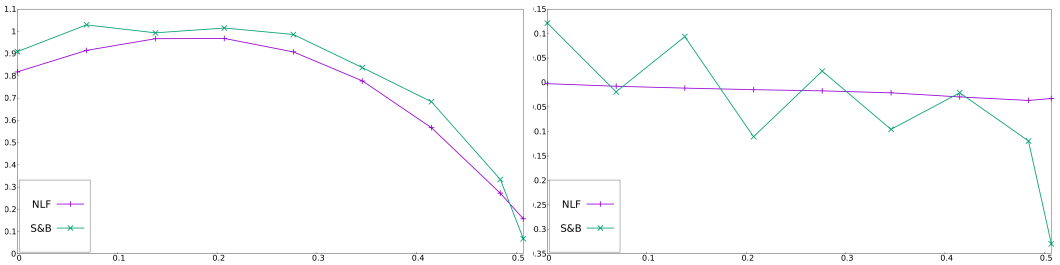

Fig. 4.10: Mean streamwise (left) and spanwise (right) velocity at $y = 22.5$

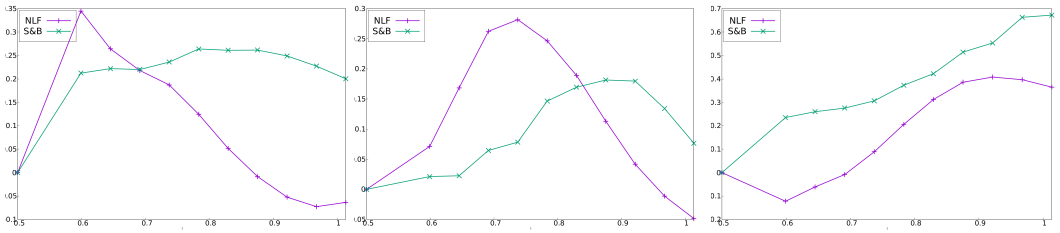

Fig. 4.11: Mean streamwise (left), shear (middle) and spanwise (right) Reynolds stresses at $x = 0$

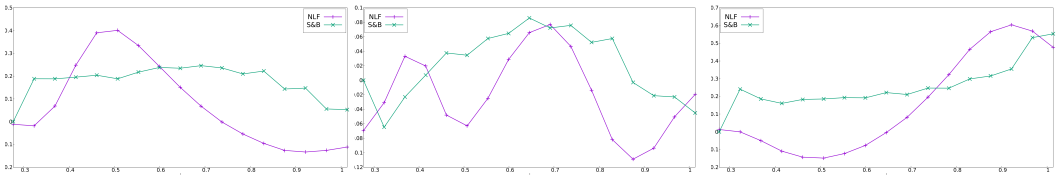

Fig. 4.12: Mean streamwise (left), shear (middle) and spanwise (right) Reynolds stresses at $x = 11$

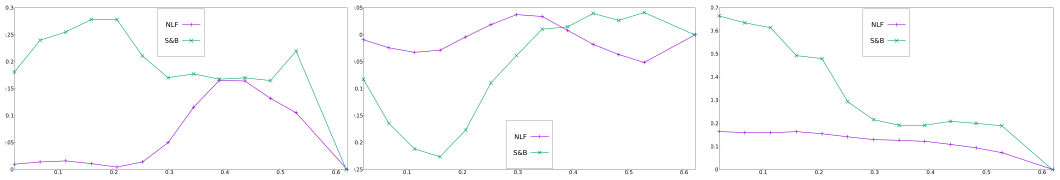

Fig. 4.13: Mean streamwise (left), shear (middle) and spanwise (right) Reynolds stresses at $x = 16.5$

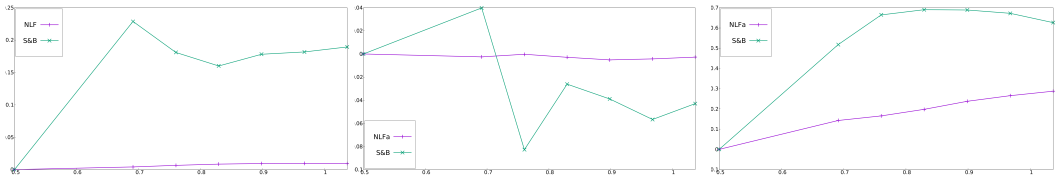

Fig. 4.14: Mean streamwise (left), shear (middle) and spanwise (right) Reynolds stresses at $y = 0$

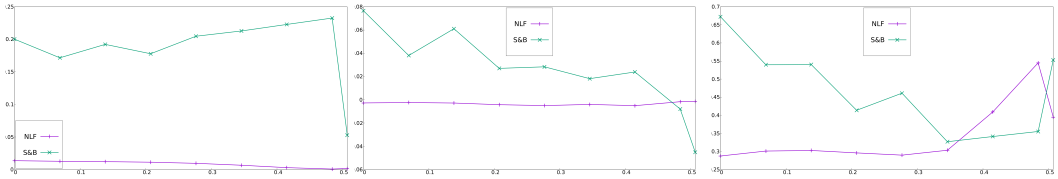

Fig. 4.15: Mean streamwise (left), shear (middle) and spanwise (right) Reynolds stresses at $y = 22.5$

The first author would like to acknowledge the support, under a Seed Research Project no. 21021440101, of University of Sharjah.

Data Availability Statement. Data sharing is not applicable to this article as no new data were created or analyzed in this study.

REFERENCES

[1] Lozovskiy A. and A. Takhirov, *Computationally efficient modular nonlinear filter stabilization for high reynolds number flows*, Adv. Comput. Math., 81 (2017), pp. 463–488.

[2] D.N. Arnold and J. Qin, *Quadratic velocity/linear pressure Stokes elements*, in Advances in Computer Methods for Partial Differential Equations VII, R. Vichnevetsky, D. Knight, and G. Richter, eds., IMACS, 1992, pp. 28–34.

[3] S. Benhamadouche and D. Laurence, *Les, coarse les, and transient rans comparisons on the flow across a tube bundle*, International Journal of Heat and Fluid Flow, 24 (2003), pp. 470 – 479. Selected Papers from the Fifth International Conference on Engineering Turbulence Modelling and Measurements.

[4] C. Benocci and A. Pinelli, *The role of the forcing term in the large eddy simulation of equilibrium channel flow*, in International Symposium On Engineering Turbulence Modelling And Measurements, Dubrovnik, Yugoslavia, Sep 24-28, 1990, 1990.

[5] L.C. Berselli, T. Iliescu, and W.J. Layton, *Mathematics of Large Eddy Simulation of Turbulent Flows*, Springer, Berlin, 2006.

[6] L. Bertagna, A. Quaini, and A. Veneziani, *Deconvolution-based nonlinear filtering for incompressible flows at moderately large Reynolds numbers*, Int. J. Numer. Meth. Fluids, 81 (2016), pp. 463–488.

[7] J. Boussinesq, *Essai sur la theories des eaux courantes*, 1877.

[8] A. Bowers, L. Rebholz, A. Takhirov, and C. Trenchea, *Improved accuracy in regularization models of incompressible flow via adaptive nonlinear filtering*, Int. J. Numer. Meth. Fluids, 70 (2012), pp. 805–828.

[9] Abigail L. Bowers and Leo G. Rebholz, *Numerical study of a regularization model for incompressible flow with deconvolution-based adaptive nonlinear filtering*, Comp. Meth. Appl. M., 258 (2013), pp. 1 – 12.

[10] John P. Boyd, *Two comments on filtering (artificial viscosity) for chebyshev and legendre spectral and spectral element methods: Preserving boundary conditions and interpretation of the filter as a diffusion*, Journal of Computational Physics, 143 (1998), pp. 283 – 288.

[11] David L. Brown, *Performance of under-resolved two-dimensional incompressible flow simulations*, Journal of Computational Physics, 122 (1995), pp. 165 – 183.

[12] Y. Cao, E.M. Lunasin, and E.S. Titi, *Global well-posedness of three-dimensional viscous and inviscid simplified Bardina turbulence models*, Commun. Math. Sci., 4 (2006), pp. 823–848.

[13] Paul Fischer and Julia Mullen, *Filter-based stabilization of spectral element methods*, Comptes Rendus de l'Académie des Sciences - Series I - Mathematics, 332 (2001), pp. 265 – 270.

[14] Jean-Luc Guermond, *On the use of the notion of suitable weak solutions in CFD*, Int. J. Numer. Meth. Fluids, 57 (2008), pp. 1153–1170.
[15] Jean-Luc Guermond and P. D. Minev, *High-order time stepping for the incompressible Navier-Stokes equations*, SIAM J. Sci. Comput., 37 (2015), pp. A2656–A2681.
[16] ———, *High-order time stepping for the Navier-Stokes equations with minimal computational complexity*, J. Comput. Appl. Math., 310 (2017), pp. 92 – 103. Numerical Algorithms for Scientific and Engineering Applications.
[17] Jean-Luc Guermond, P. D. Minev, and J. Shen, *An overview of projection methods for incompressible flows*, Comp. Meth. Appl. M., 195 (2006), pp. 6011 – 6045.
[18] Jean-Luc Guermond, T.J. Oden, and S. Prudhomme, *Mathematical perspectives on Large Eddy Simulation models for turbulent flows*, J. Math. Fluid Mech., 6 (2004), pp. 194–248.
[19] Jean-Luc Guermond, R. Pasquetti, and B. Popov, *From suitable weak solutions to entropy viscosity*, J. Sci. Comput., 49 (2011), pp. 35–50.
[20] Y.A. Hassan and H.R. Barsamian, *Tube bundle flows with the large eddy simulation technique in curvilinear coordinates*, International Journal of Heat and Mass Transfer, 47 (2004), pp. 3057 – 3071.
[21] F. Hecht, *New development in FreeFem++*, J. Numer. Math., 20 (2012), pp. 251–265.
[22] Nan Jiang and William Layton, *Algorithms and models for turbulence not at statistical equilibrium*, Computers and Mathematics with Applications, 71 (2016), pp. 2352 – 2372.
[23] Nan Jiang, William Layton, Michael McLaughlin, Yao Rong, and Haiyun Zhao, *On the foundations of eddy viscosity models of turbulence*, Fluids, 5 (2020).
[24] Richard W. Johnson, *Modeling strategies for unsteady turbulent flows in the lower plenum of the vhtr*, Nuclear Engineering and Design, 238 (2008), pp. 482 – 491. Benchmarking of CFD Codes for Application to Nuclear Reactor Safety.
[25] Mathieu Labois and Djamel Lakehal, *Very-large eddy simulation (v-les) of the flow across a tube bundle*, Nuclear Engineering and Design, 241 (2011), pp. 2075–2085. (W3MDM) University of Leeds International Symposium: What Where When? Multi-dimensional Advances for Industrial Process Monitoring.
[26] William Layton, Nathaniel Mays, Monika Neda, and Catalin Trenchea, *Numerical analysis of modular regularization methods for the BDF2 time discretization of the Navier-Stokes equations*, ESAIM-Math. Model. Num., 48 (2014), p. 765–793.
[27] William Layton, Leo G. Rebholz, and Catalin Trenchea, *Modular nonlinear filter stabilization of methods for higher Reynolds numbers flow*, J. Math. Fluid Mech., 14 (2012), pp. 325–354.
[28] William Layton and Aziz Takhirov, *Numerical analysis of wall adapted nonlinear filter models of turbulent flows*, Contemp. Math., 586 (2013), pp. 219 – 229.
[29] Michael L. Minion and David L. Brown, *Performance of under-resolved two-dimensional incompressible flow simulations, ii*, Journal of Computational Physics, 138 (1997), pp. 734 – 765.
[30] Julie S. Mullen and Paul F. Fischer, *Filtering techniques for complex geometry fluid flows*, Communications in Numerical Methods in Engineering, 15 (1999), pp. 9–18.
[31] M. Olshanskii and X. Xiong, *A connection between filter stabilization and eddy viscosity models*, Numer. Meth. Part.l D. E., 29 (2013), pp. 2061–2080.
[32] Stephen B. Pope, *Turbulent Flows*, Cambridge University Press, 2000.
[33] Artit RIDLUAN and Akira TOKUHIRO, *Benchmark simulation of turbulent flow through a staggered tube bundle to support cfd as a reactor design tool. part i: Srans cfd simulation*, Journal of Nuclear Science and Technology, 45 (2008), pp. 1293–1304.
[34] ———, *Benchmark simulation of turbulent flow through a staggered tube bundle to support cfd as a reactor design tool. part ii: Urans cfd simulation*, Journal of Nuclear Science and Technology, 45 (2008), pp. 1305–1315.
[35] P. Rollet-Miet, D. Laurence, and J. Ferziger, *Les and rans of turbulent flow in tube bundles*, International Journal of Heat and Fluid Flow, 20 (1999), pp. 241 – 254.
[36] O. Simonin and M. Barcouda, *Measurements of fully developed turbulent flow across tube bundle*, in Proceedings of the Third International Sym posium on Applications of Laser Anemometry to Fluid Mechanics, Lisbon, Portugal, 1986.
[37] ———, *Measurements and prediction of turbulent flow entering a staggered tube bundle*, in Fourth International Symposium on Applications of Laser Anemometry to Fluid Mechanics paper 5.23, Lisbon, Portugal, 1988.
[38] Aziz Takhirov, *Voigt regularization for the explicit time stepping of the Hall effect term*, Geophys. Astro. Fluid., 110 (2016), pp. 409–431.
[39] Alex Viguerie and Alessandro Veneziani, *Deconvolution-based stabilization of the incompressible navier–stokes equations*, Journal of Computational Physics, 391 (2019), pp. 226 – 242.
[40] Huijuan Xu, Davide Baroli, Francesca Di Massimo, Annalisa Quaini, and Alessandro Veneziani, *Backflow stabilization by deconvolution-based large eddy simulation modeling*, Journal of Computational Physics, 404 (2020), p. 109103.